



HAL
open science

Three-Dimensional CFD Analysis of a Hot Water Storage Tank with Various Inlet/Outlet Configurations

Alina Abdidin, Abzal Seitov, Amankeldy Toleukhanov, Yerzhan Belyayev,
Olivier Botella, Abdelhamid Kheiri, Mohammed Khalij

► **To cite this version:**

Alina Abdidin, Abzal Seitov, Amankeldy Toleukhanov, Yerzhan Belyayev, Olivier Botella, et al.. Three-Dimensional CFD Analysis of a Hot Water Storage Tank with Various Inlet/Outlet Configurations. *Energies*, 2024, 17, pp.5716. 10.3390/en17225716 . hal-04847936

HAL Id: hal-04847936

<https://hal.univ-lorraine.fr/hal-04847936v1>

Submitted on 19 Dec 2024

HAL is a multi-disciplinary open access archive for the deposit and dissemination of scientific research documents, whether they are published or not. The documents may come from teaching and research institutions in France or abroad, or from public or private research centers.






L'archive ouverte pluridisciplinaire **HAL**, est destinée au dépôt et à la diffusion de documents scientifiques de niveau recherche, publiés ou non, émanant des établissements d'enseignement et de recherche français ou étrangers, des laboratoires publics ou privés.



Distributed under a Creative Commons Attribution 4.0 International License

Article

Three-Dimensional CFD Analysis of a Hot Water Storage Tank with Various Inlet/Outlet Configurations

Alina Abdidin ^{1,2}, Abzal Seitov ¹, Amankeldy Toleukhanov ^{3,*}, Yerzhan Belyayev ^{1,*}, Olivier Botella ²,
Abdelhamid Kheiri ² and Mohammed Khalij ²

¹ Department of Mechanics, Al-Farabi Kazakh National University, Almaty 050040, Kazakhstan

² Université de Lorraine, CNRS, LEMTA, F-54000 Nancy, France

³ Department of Mechanical Engineering, Satbayev University, Almaty 050013, Kazakhstan

* Correspondence: aman.toleukhanov@gmail.com (A.T.); yertzhan.belyayev@kaznu.edu.kz or yertzhan.belyayev@gmail.com (Y.B.); Tel.: +7-771-491-3344 (Y.B.)

Abstract: This study presents a comprehensive 3D numerical analysis of thermal stratification, fluid dynamics, and heat transfer efficiency across six hot water storage tank configurations, identified as Tank-1 through Tank-6. The objective is to determine the most effective design for achieving uniform temperature distribution, stable stratification, and efficient heat retention in sensible heat storage systems, with potential for integration with phase change materials (PCMs). Using COMSOL Multiphysics 5.6, simulations were conducted to evaluate key performance indicators, including the Richardson number, capacity ratio, and exergy efficiency. Among the tanks, Tank-1 demonstrated the highest efficiency, with a capacity ratio of 84.6% and an exergy efficiency of 72.5%, while Tank-3, which achieved a capacity ratio of 70.2% and exergy efficiency of 50.5%, was identified as the most practical for real-world applications due to its balanced heat distribution and feasibility for PCM integration. Calculated dimensionless numbers (Reynolds number: 635, Prandtl number: 4.5, and Peclet number: 2858) indicated laminar flow and dominant convective heat transfer across all the configurations. These findings provide valuable insights into the design of efficient thermal storage systems, with Tank-3's configuration offering a practical balance of thermal performance and operational feasibility. Future work will explore the inclusion of PCM containers within Tank-3, as well as applications for heat pump and solar water heaters, and high-temperature heat storage with various working fluids.

Keywords: sensible heat storage; CFD simulation; inlet/outlet configurations; water storage tank; performance indicators



Citation: Abdidin, A.; Seitov, A.; Toleukhanov, A.; Belyayev, Y.; Botella, O.; Kheiri, A.; Khalij, M. Three-Dimensional CFD Analysis of a Hot Water Storage Tank with Various Inlet/Outlet Configurations. *Energies* **2024**, *17*, 5716. <https://doi.org/10.3390/en17225716>

Academic Editor: Kwok Tong Chau

Received: 10 October 2024

Revised: 7 November 2024

Accepted: 13 November 2024

Published: 15 November 2024



Copyright: © 2024 by the authors. Licensee MDPI, Basel, Switzerland. This article is an open access article distributed under the terms and conditions of the Creative Commons Attribution (CC BY) license (<https://creativecommons.org/licenses/by/4.0/>).

1. Introduction

Thermal energy storage plays a pivotal role in enhancing the efficiency and flexibility of energy systems, particularly in applications such as heating [1], cooling [2], and renewable energy integration [3]. There are two primary methods for thermal energy storage: sensible heat storage (SHS) [4] and latent heat storage (LHS) using phase change materials (PCM) [5]. Sensible heat storage relies on raising or lowering the temperature of a storage medium, such as water [6], to store or release energy. This method is simple and widely used but often requires large volumes to store significant amounts of energy, as it depends on the temperature difference of the medium.

In contrast, latent heat storage with PCMs capitalizes on the phase transition of materials, from solid to liquid or vice versa, to store and release large amounts of energy in a compact space [5]. PCM-based systems offer higher energy storage density [7] and can maintain nearly constant temperatures during the phase transition, making them advantageous for applications requiring stable thermal conditions. However, the integration of PCMs in storage tanks introduces complexities in design and operation, particularly

in managing heat transfer and ensuring uniform phase transitions throughout the storage medium.

This study compares six different storage tank configurations, assessing both sensible heat storage tanks and their potential to be adapted for use with PCM-based latent heat storage. Through a detailed numerical analysis, this research aims to evaluate the thermal performance of these configurations, focusing on parameters such as thermal stratification [8], mixing behavior [6], and overall heat retention [9] efficiency. By examining SHS tanks with different inlet and outlet nozzle configurations, this research aims to provide insights for optimizing thermal storage systems for future LHS applications.

To achieve this, it is essential to ensure uniform temperature distribution within the tank, where containers or capsules with PCMs are placed. This will minimize thermal stratification, thereby improving the charging and discharging processes of the thermal storage system. One of the key tools for studying this process is computational fluid dynamics (CFD) [4,10], which allows for the examination of a wide range of geometric configurations without the need for time-consuming and labor-intensive experiments.

Chekifi and Boukraa [4] reviewed a range of studies that utilized CFD to evaluate SHS configurations, addressing topics such as flow behavior, heat transfer mechanisms, and material compatibility. Additionally, their work explored the integration of SHS systems with renewable energy applications. For modeling the charging and discharging processes of sensible heat storage tanks, 2D solvers were predominantly used, either developed in an in-house CFD code or utilizing built-in algorithms within software packages. Hosseinnia et al. [11] investigated the thermocline formation and its evolution within a thermal energy storage (TES) tank during the charging process. The study utilized a 2D CFD model, implemented using ANSYS Fluent, to simulate the charging phase and analyze the thermocline thickness (TLT)—a key indicator of thermal stratification performance. The paper proposes a new criterion for quantifying TLT and explores how diffuser designs, tank geometry, and heat loss impact the thermocline's development. Bouhal et al. [12] investigated the effects of flat plate positions and orientations on thermal stratification in solar water storage tanks. Using 2D CFD simulations implemented in ANSYS Fluent, the study evaluated temperature distribution, flow dynamics, and the effectiveness of thermal stratification. The authors concluded that positioning flat plates at different heights within the tank can significantly affect stratification, with optimal performance achieved when the plate was placed at the middle height of the tank. Additionally, varying the tilt angles of the plates improved the thermocline structure, enhancing the overall thermal performance. These findings provide insights for optimizing solar water heating systems by fine-tuning the design of storage tanks. Fertahi et al. [13] investigated the thermal performance of a horizontal hot water storage tank used in evacuated tube collector (ETC) solar water heaters. Using a combination of experimental studies and 2D CFD simulations with OpenFOAM, the paper explores the impact of varying the number of heat pipes on the tank's energy performance. The study focused on optimizing the heat transfer coefficient (HTC), temperature distribution, and discharging efficiency. The results demonstrate that increasing the number of heat pipes enhanced the heat transfer rate but also disturbed the flow patterns within the tank, leading to fluctuations in temperature and efficiency. These findings provide valuable insights for optimizing the design of horizontal storage tanks in ETC solar water heating systems. Lou et al. [14] investigated the impact of an optimized flow distributor design on thermal stratification within a single-medium thermocline (SMT) storage tank. Using both 2D CFD simulations in ANSYS Fluent and experimental validation, the study proposed a ring-opening plate distributor (ROPD) to minimize thermocline degradation and improve charging and discharging efficiency. The results show that the optimized ROPD improves the charging efficiency by up to 14.5% and discharging efficiency by 19.8%, providing valuable insights for designing more efficient thermal energy storage systems. The study highlights the importance of flow rate, temperature difference, and inlet configurations in maintaining thermal stratification and energy efficiency. Kumar and Singh [15] examined the thermal performance of a domestic hot water storage tank under different dynamic

operating modes—charging, continuous delivery, and discharging. Using 2D CFD simulations in ANSYS Fluent, the study focused on the degree of thermal stratification achieved in each operating mode. The results show that thermal stratification improved when the heat exchanger was located in the upper part of the tank during charging and continuous delivery. The paper highlights that optimal tank design and placement of heat exchangers can significantly enhance thermal performance, reducing energy losses.

Most CFD simulations are predominantly conducted on 2D models. According to the aforementioned review, a significant portion of this 2D analysis focuses on tanks with modified internal structures and varied inlet/outlet conditions. Utilizing commercial solvers is a practical approach, particularly as further modifications to TES tanks involve complex geometries, where 3D effects become significant. However, there is a limited number of studies dedicated to the 3D numerical analysis of such tanks. A few notable examples of these studies are presented below.

Shafieian et al. [16] investigated the impact of various inlet configurations on the thermal performance of solar hot water storage tanks. The study used 3D unsteady CFD simulations with ANSYS Fluent to analyze various tank designs, including a single inlet/outlet configuration, a dual inlet design, and the use of diffusers with varying aspect ratios. The results show that higher mass flow rates tend to degrade thermal stratification, while the use of diffusers and optimized inlet configurations can improve thermal performance by reducing unwanted mixing. The study highlights that smaller diffuser aspect ratios (between 1.0 and 1.5) are most effective in maintaining stratification. The primary focus of this study is on the configuration of a single inlet and outlet, with specific application to solar water heating systems, albeit exploring a limited range of inlet/outlet arrangements. Kong et al. [17] presented a 3D transient CFD study using ANSYS Fluent, focusing on improving thermal stratification in water storage tanks. The paper investigates the use of an inner cylinder with openings as a diffuser to enhance stratification and maintain a stable thermocline during the charging process. The simulation results, validated with experimental data, show that the inner cylinder design effectively reduced turbulence, improved heat transfer efficiency, and increased the thermal stratification performance of the tank. The primary focus here is on the modification of the internal geometry of the tank, while the numerical model and algorithm are only briefly discussed. Wang et al. [18] focused on the optimization of thermal stratification in a thermal diode tank (TDT) for cold energy storage using 3D ANSYS Fluent-based CFD simulations. The study investigated different TDT designs, including the use of obstacles, to enhance the stratification and improve the performance of a refrigeration and air-conditioning (RAC) system. The key findings show that a vertical orientation of the tank and optimized obstacle configurations significantly improved system efficiency, with thermal stratification boosting the coefficient of performance (COP) by up to 10%. The research provides insights for designing more efficient TDT systems for energy-saving applications in RAC systems. Shaikh et al. [19] focused on the numerical analysis of thermocline thickness in SMTs used for thermal energy storage, particularly in concentrated solar power (CSP) plants. Using 3D COMSOL Multiphysics, the study investigated various parameters, such as the Peclet number, Atwood number, and inlet configurations, to assess their impact on thermal stratification and tank performance. The results demonstrate that the introduction of a porous vertical flow distributor reduced thermocline thickness, thus improving thermal stratification. In this study, a porous distributor is located inside the tank, and only a single inlet and outlet configuration for the solar water heating system is considered. Experimental validation is not provided; instead, comparisons are made with the numerical results from other authors.

The presented literature review indicates that ANSYS Fluent is predominantly used as the numerical tool for CFD studies of charging and discharging efficiency in SHS hot water tanks, with OpenFOAM and COMSOL Multiphysics being used less frequently. Most of the studies employed 2D simulations to explore modifications to the internal geometry of tanks to either maintain thermal stratification or achieve uniform heating. The research has primarily focused on improving the charging and discharging performance

of thermal storage in solar water heaters, with limited attention given to tanks utilizing PCMs. Additionally, the literature addresses a limited number of performance indicators.

The novelty of this study lies in its use of a validated 3D COMSOL Multiphysics model to examine six configurations of inlet and outlet nozzles, aimed at improving the efficiency of SHS tanks and addressing gaps in the literature regarding 3D simulations, performance indicators, and future applications in PCM utilization. The mathematical model and 3D numerical algorithm performed with COMSOL Multiphysics 5.6 [20] will be fully described. This 3D computational tool was validated by comparing the results with experimental data and calculations from other authors, as found in the open literature. This tool will enable future investigations of various configurations for both SHS and LHS tanks.

2. Physical Model

The geometry of the inlet and outlet for the heat transfer fluid in a hot water storage tank plays a crucial role in both the charging and discharging conditions, as well as in the overall flow distribution within the tank. These factors significantly impact the tank's thermal efficiency, energy storage capacity, and system performance. During the charging phase, where the tank is filled with heated fluid, the inlet geometry determines how the heat transfer fluid enters the tank. An optimally designed inlet ensures that the hot fluid is evenly distributed throughout the tank, promoting uniform temperature distribution and reducing the risk of thermal stratification. A well-distributed flow at the inlet prevents hot spots and ensures that the stored energy is maximized, leading to more efficient use of the storage capacity. In the discharging phase, where hot water is drawn from the tank, the outlet geometry becomes critical. A properly designed outlet allows for smooth and controlled extraction of hot water while minimizing disturbances to the thermal layers within the tank. If the outlet geometry is not optimized, it can cause unwanted mixing of the hot and cold layers, reducing the efficiency of heat extraction and leading to uneven temperatures in the outgoing fluid. The overall flow distribution within the tank is influenced by both the inlet and outlet geometries. Properly designed inlet and outlet configurations help maintain thermal stratification, where the hottest water remains at the top of the tank and the cooler water settles at the bottom. This stratification is essential for efficient energy use, as it allows for the extraction of the hottest water during discharging while maintaining a reserve of cooler water. In both charging and discharging conditions, the geometry of the inlets and outlets helps minimize energy losses. For example, diffusers or flow guides at the inlet can help spread the fluid more evenly, preventing turbulence and ensuring that the fluid flows smoothly across the entire tank. Similarly, the outlet design can reduce the risk of backflow or short-circuiting, where incoming and outgoing fluids mix prematurely. In renewable energy systems, such as solar thermal storage, the inlet and outlet geometries may need to adapt to varying flow rates and temperatures. Efficient designs ensure that the tank can handle these variations without significant losses in performance. For example, in solar thermal applications, the tank must efficiently store and release energy according to the availability of solar input and the demand for hot water. By carefully designing the inlet and outlet geometries, engineers can optimize the overall performance of the hot water storage system. This includes maximizing heat retention, improving energy efficiency, and ensuring a consistent hot water supply even under varying demand conditions.

As stated in the Introduction, this paper examines a hot water storage tank utilizing sensible heat storage. These studies serve as preliminary calculations for future applications in thermal storage tanks incorporating phase change materials. The primary objective of this study is to investigate the impact of inlet/outlet geometrical configurations on the distribution of heat transfer fluid (HTF) within a heat storage tank. To achieve this, the six different inlet and outlet configurations presented in Figure 1 were considered. The configurations in this figure are the following: (a) Tank-1—top and bottom open inlet/outlet, (b) Tank-2—top and bottom one nozzle inlet/outlet, (c) Tank-3—top and bottom multiple nozzle inlet/outlet, (d) Tank-4—one side, one nozzle inlet/outlet, (e) Tank-5—two sides, one nozzle inlet/outlet, (f) Tank-6—side multiple nozzle inlet/outlet.

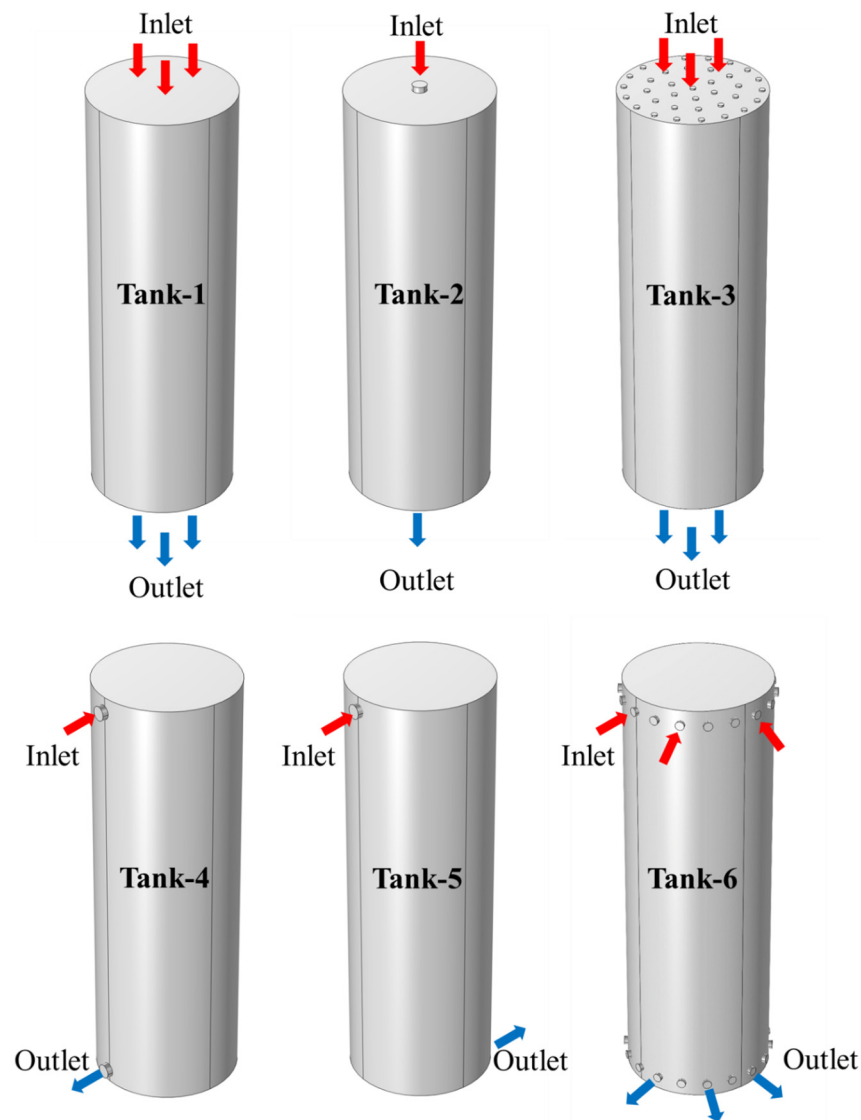


Figure 1. Schematic configurations of the storage tanks with different inlet and outlet configurations.

The external tank dimensions are the same for all six configurations: the tank height is $H = 3.0$ m, and the diameter is $D = 1.0$ m. Detailed dimensions of the inlet and outlet nozzles for the six tanks are provided in Table 1. Tank-1 has fully open top and bottom sections. Tank-2 has one opening in the top section and one in the bottom section, each with a diameter of 0.1 m. Tank-3 has 37 nozzles on the top cover and 37 nozzles on the bottom cover, each with a diameter of 0.04 m. Tank-4 and Tank-5 differ only in the location of the inlet and the outlet: either on the same (Tank-4) or opposite sides (Tank-5), with the same opening diameter of 0.1 m. Tank-6 has 18 nozzles on the upper side and 18 nozzles on the lower side, each with a diameter of 0.06 m. Both charging and discharging modes of the heat accumulation tank are considered. During charging, the inlet is positioned at the top of the tank and the outlet is at the bottom. Conversely, the inlet is at the bottom, and the outlet is at the top for discharging. There are two extreme temperatures: $60\text{ }^{\circ}\text{C}$ for the hot HTF (T_h) and $20\text{ }^{\circ}\text{C}$ for the cold HTF (T_c), with water as the working fluid. During charging, the inlet water temperature (T_{in}) is $60\text{ }^{\circ}\text{C}$, while the initial temperature (T_{ini}) of the water in the tank is $20\text{ }^{\circ}\text{C}$. Conversely, during discharging, the T_{in} is $20\text{ }^{\circ}\text{C}$, and the T_{ini} in the tank is $60\text{ }^{\circ}\text{C}$. All the configurations use the same volume flow rate of $0.000327\text{ m}^3/\text{s}$ for the HTF. Due to the different inlet configurations, the HTF velocities will vary, although the flow rate remains constant. The tank walls are made of stainless steel and are assumed to be perfectly insulated, with no heat loss.

Table 1. Geometries and operating conditions.

Diameter D (m)	1	
Height H (m)	3	
Nº	Inlet/outlet nozzle diameter d (m)	Number of inlet/outlet nozzles
Tank-1	1	1
Tank-2	0.1	1
Tank-3	0.04	37
Tank-4	0.1	1
Tank-5	0.1	1
Tank-6	0.06	18
Hot temperature T_h (°C)	60	
Cold temperature T_c (°C)	20	
Flow rate Q_{in} (m ³ /s)	0.000327	

3. Mathematical Model

3.1. CFD Model

This section outlines the fundamental assumptions and equations that form the basis for simulating heat transfer and fluid flow within a hot water storage tank. By establishing key assumptions, the model aims to accurately represent the system's behavior under various configurations, with particular emphasis on different inlet/outlet designs in 3D storage tanks. The following sections detail the foundational assumptions guiding the mathematical formulation, followed by the specific equations used to model the system's transient thermal and fluid dynamics.

The unsteady, three-dimensional flow models for heat transfer within a conventional storage tank are based on the following assumptions:

- The working fluid is treated as incompressible.
- The thermophysical properties of the fluid are considered constant, except for density variations due to temperature changes, which are accounted for using the Boussinesq approximation to model thermal buoyancy effects.
- The fluid is assumed to be Newtonian.
- Fluid motion is assumed to be laminar and three-dimensional.

The transient thermal and fluid dynamics are described by the three-dimensional forms of the Navier–Stokes equations and the energy equation, incorporating the effects of gravity. Accordingly, the governing equations are formulated based on these assumptions.

The HTF is described by the system of 3D Navier–Stokes equations for an incompressible fluid. The continuity is described by Equation (1):

$$\nabla \cdot \vec{u} = 0, \quad (1)$$

where the velocity vector \vec{u} has three components in cylindrical coordinates: (u_r, u_θ, u_z) .

The following equation describes the conservation of momentum in vector form:

$$\frac{\partial \vec{u}}{\partial t} + (\vec{u} \cdot \nabla) \vec{u} = -\frac{1}{\rho_f} \nabla p_f + \nu_f \nabla^2 \vec{u} + \beta \Delta T \vec{g} \quad (2)$$

Here, the index f —is an indicator of the HTE, ρ_f is the fluid density, ν_f is the fluid kinematic viscosity, \vec{g} is the gravity, β is the coefficient of thermal expansion, and gravity is considered in the direction z .

The energy equation describing the heat exchange process is defined as follows:

$$\rho_f C_{p_f} \frac{\partial T}{\partial t} + \rho_f C_{p_f} \vec{u} \cdot \nabla T = \nabla(k \nabla T), \quad (3)$$

where T is the temperature, C_{p_f} is the specific heat capacity at constant pressure, and k is the thermal conductivity.

3.2. Initial and Boundary Conditions

This subsection outlines the parameters and constraints implemented in the model to ensure accurate and realistic simulations. The initial conditions define the system's starting state, including temperature distributions and fluid velocities, while the boundary conditions establish constraints at the boundaries of the computational domain. These conditions collectively provide the framework for solving the governing equations, ensuring that the model accurately represents the physical behavior of the system under investigation. This section is essential for configuring the simulation and obtaining reliable results that are consistent with experimental or theoretical expectations.

For fluid flow, boundary conditions (BC) are applied to solid surfaces, including the tank walls and the walls of the inlet/outlet nozzles. Additionally, it is assumed that the storage tank is fully insulated, which is represented by the following formula:

$$-\vec{n}(-k \nabla T) = 0 \quad (4)$$

where \vec{n} is the normal vector to the heat transfer surface. Thus, heat transfer is carried out only with the help of inlet and outlet pipes.

A no-slip boundary condition is applied for the velocity components at the walls:

$$u_r = u_\theta = u_z = 0, \quad (5)$$

The initial temperature of the water (T_{ini}) is calculated as follows:

$$T(r, \theta, z, t = 0) = T_{ini}, \quad (6)$$

where T_{ini} is the initial temperature of the water throughout the tank.

$$T_{ini} = \begin{cases} 20 \text{ }^\circ\text{C} & \text{for charging,} \\ 60 \text{ }^\circ\text{C} & \text{for discharging} \end{cases} \quad (7)$$

The initial velocity in the tank is zero in all cases.

The inlet temperature for the charging and discharging modes is as follows:

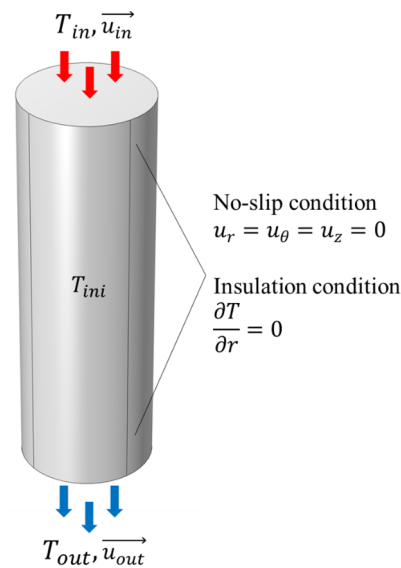
$$T_{in} = \begin{cases} 60 \text{ }^\circ\text{C} & \text{for charging,} \\ 20 \text{ }^\circ\text{C} & \text{for discharging} \end{cases} \quad (8)$$

The inlet velocities are defined according to Table 2. The inlet water velocity is calculated based on a flow rate of $Q_{in} = 0.000327 \text{ m}^3/\text{s}$ for each configuration. A zero-pressure boundary condition is applied at the outlet.

The diagram in Figure 2 corresponds to the Tank-1 configuration, as shown in Figure 1. For the remaining five configurations, similar initial and boundary conditions are applied, with consideration given to the presence of perforated walls on the lid and at the bottom of the tank.

Table 2. Inlet velocities.

Inlet velocity u_{zin}	Tank-1: 0.000416 m/s
	Tank-2: 0.0416 m/s
	Tank-3: 0.00704 m/s
	Tank-4: 0.0416 m/s
	Tank-5: 0.0416 m/s
	Tank-6: 0.00643 m/s

**Figure 2.** Schematic representation of initial and boundary conditions for Tank-1.

3.3. Performance Indicators

The performance of the thermal energy storage system can be evaluated using two primary methodologies: graphical (visual) techniques and performance indicator (quantitative) approaches. Graphical techniques, such as CFD analysis, involve examining temperature and velocity contours within the storage tank, providing detailed insights into the local thermal and fluid dynamics. Although these techniques offer valuable visual information, they do not provide direct quantitative assessments of the system's overall performance. Conversely, the performance indicator approach involves calculating specific metrics to assess the system's operational efficiency and effectiveness quantitatively. For a comprehensive evaluation of the system's performance, it is crucial to integrate both graphical analysis and performance indicators, thereby enabling a thorough assessment of the system's behavior and effectiveness.

According to the literature, performance indicators for thermal energy storage systems can be categorized according to their underlying thermodynamic principles [21]. Indicators associated with the first law of thermodynamics quantify the total amount of thermal energy stored, reflecting the overall energy balance within the system. In contrast, indicators related to the second law of thermodynamics evaluate the quality of the stored energy, offering insights into the efficiency and effectiveness of the storage process. This distinction between the two categories of indicators enables a more comprehensive assessment of both the quantity and quality of the stored thermal energy.

The capacity ratio (σ) quantifies the fraction of the total thermal energy (E_{stored}^V) retained at the conclusion of the charging phase relative to the system's maximum thermal energy storage capacity (E_{max_stored}) [9]:

$$\sigma = \frac{E_{stored}^V}{E_{max_stored}}, \quad (9)$$

$$E_{stored}^V = \int_V \rho_f C_{p_f} (T - T_c) dV, \quad (10)$$

$$E_{max_stored} = \rho_f C_{p_f} V_{tank} (T_h - T_c), \quad (11)$$

where T_c (or T_{ini}) is the initial water temperature in the tank, T is the local water temperature, T_h (or T_{in}) is the final uniform water temperature along the height of the tank, and V_{tank} is the volume of the storage tank.

By applying the principles of the first and second laws of thermodynamics, exergy quantifies both the quantity and quality of the thermal energy stored in storage tanks [22]. The exergy of a sensible heat storage tank quantifies the potential to do work based on the thermal energy stored and the temperature difference relative to the ambient environment. In Ref. [23], exergy efficiency is defined as the ratio of the actual exergy of the storage tank at the end of the charging process to the ideal exergy that the tank could have achieved under ideal conditions at the same point in time:

$$\eta_{exergy} = \frac{Exergy_{real}}{Exergy_{ideal}} \Big|_{at\ the\ end\ of\ charging\ process}, \quad (12)$$

$$Exergy_{real} = \int_V \rho_f C_{p_f} (T - T_a) dV - \int_V \rho_f C_{p_f} T_a \ln\left(\frac{T}{T_a}\right) dV, \quad (13)$$

$$Exergy_{ideal} = \rho_f C_{p_f} V_{tank} \left[(T_h - T_a) - T_a \ln\left(\frac{T_h}{T_a}\right) \right], \quad (14)$$

where T_a is the ambient temperature.

The charging (η_{ch}) and discharging (η_{dis}) efficiencies are calculated using the following equations:

$$\eta_{ch} = \frac{\Delta E}{\Delta E_h}, \quad (15)$$

$$\eta_{dis} = \frac{\Delta E}{\Delta E_c}, \quad (16)$$

where ΔE_h and ΔE_c represent the total energy flow during the charging and discharging cases, respectively. These values are determined using the following equations:

$$\Delta E_h = \int_0^{t_f} \dot{m}_f C_{p_f} (T_h - T_{ini}) dt, \quad (17)$$

$$\Delta E_c = \int_0^{t_f} \dot{m}_f C_{p_f} (T_{ini} - T_c) dt, \quad (18)$$

where \dot{m}_f is the mass flow rate.

The energy accumulated in the TES at time t , denoted as ΔE , is the difference between the initial energy content of the storage system and the energy content at time t , expressed by the following equation:

$$E = \int_0^{t_f} \rho_f C_{p_f} (\bar{T} - T_{ini}) dt, \quad (19)$$

where \bar{T} is the average temperature along the height of the tank.

The theoretical charging/discharging time of the storage tank is defined as the fluid residence time, assuming plug flow conditions. It is calculated as the ratio of the total tank volume ($V_{tank} = 2.3 \text{ m}^3$) to the charging/discharging volume flow rate (Q_{in}) and is given by the following equation:

$$t_{ch} = \frac{V_{tank}}{Q_{in}}, \quad (20)$$

Another parameter is the Richardson number (Ri) for the storage tank, which indicates the relationship between natural and forced convection in the liquid. It is defined as the

ratio of the potential energy associated with temperature stratification to the kinetic energy associated with fluid motion. This number is used to evaluate the degree of stratification in storage tanks: a high Richardson number indicates the dominance of natural convection and good stratification, while a low value indicates the dominance of forced convection and more uniform mixing of the liquid.

The Richardson number is calculated using the following formula:

$$Ri = \frac{g\beta H(T_{top} - T_{bottom})}{u_{zin}^2}. \quad (21)$$

where T_{top} and T_{bottom} are the temperatures at the top and bottom of the tank, respectively. These temperatures are calculated as averages over these top and bottom sections. The Richardson number is calculated at each time step.

Another important parameter is the Peclet number, a dimensionless value used in fluid mechanics and heat or mass transfer. It describes the relative significance of advection (transport caused by fluid motion) compared to diffusion (spreading due to concentration or temperature gradients). Specifically, it helps assess how effectively heat is transported through the tank by fluid motion versus how much heat is lost or gained through conduction within the fluid. Additional dimensionless parameters characterizing the flow of a viscous incompressible fluid with heat transfer include the Reynolds and Prandtl numbers. From these two quantities, the Peclet number can also be determined. The commonly known equations for their calculation are as follows:

$$Pe = \frac{4Q_{in}}{\pi \cdot D \cdot \alpha}, \quad Re = \frac{4Q_{in}}{\pi \cdot D \cdot v_f}, \quad Pr = \frac{v_f}{\alpha}, \quad Pe = Re \cdot Pr, \quad \alpha = \frac{k}{\rho_f \cdot C_{p_f}}. \quad (22)$$

The characteristic length is typically the storage tank diameter D , and α is the thermal diffusivity.

4. Calculation Model

To conduct numerical simulations of the six tank configurations, the licensed software COMSOL Multiphysics 5.6 [20] was utilized. This software is designed for multiphysics simulations in complex geometries, employing advanced solvers and a user-friendly interface that enables the simultaneous solution of systems of time-dependent partial differential equations. COMSOL models physical phenomena, such as mechanics, thermodynamics, electromagnetism, chemical reactions, multiphase fluid flow, and combinations. The software facilitates the integration and interaction of multiple physical processes within a single model, making it a valuable tool for studying physical processes in modern energy systems.

To investigate the flow of the heat transfer fluid within the tanks, particularly considering the interaction between hotter and colder fluids during the charging and discharging cycles of the thermal storage system, a time-dependent 3D model was developed. The governing equations for fluid flow and heat transfer were approximated using the finite element method (FEM), which is implemented in COMSOL. The mathematical model is based on the fundamental conservation laws of mass, momentum, and energy. An incompressible fluid assumption was made, where mass conservation is expressed by the continuity Equation (1), the velocity components were determined by the Navier–Stokes Equation (2), and the energy equation is written in terms of temperature, accounting for heat transfer mechanisms. Boundary conditions were applied to model the inlet and outlet of the HTF, as well as the insulated tank walls (see Section 3.2). Simulations were performed in a transient state to capture the dynamic behavior of the heat storage process. The buoyancy effect was accounted for using the Boussinesq approximation in all six configurations. The mesh was refined iteratively to ensure the accuracy and convergence of the results. COMSOL Multiphysics' post-processing tools were used to visualize temperature distributions, velocity fields, and other relevant parameters, providing comprehensive insights into the system's thermal and hydrodynamic performance.

4.1. Mesh Parameters

COMSOL Multiphysics provides automatic mesh generation capabilities, significantly simplifying the modeling process. The software adapts the mesh based on the geometry and physics of the problem, optimizing calculation accuracy and minimizing errors. It also offers adaptive mesh refinement, which automatically increases resolution in areas with high gradients, such as boundary layers or regions with intensive heat transfer. This enhances the accuracy of the solutions without substantially increasing computational costs.

Table 3 presents the key parameters of the computational meshes for the six tanks. Mixed elements, including tetrahedral, prisms, and pyramids, were used during mesh generation. As seen in Table 3, Tank-1 has the lowest number of elements, while Tank-3 and Tank-5 have the highest. In all the configurations, most of the elements were tetrahedral, followed by prisms and pyramids. Prisms and pyramids were used near the walls, the top cover, and the bottoms of the tanks. For Tank-3 and Tank-6, which have numerous openings, a higher number of prisms and pyramids were used.

Table 3. Mesh properties.

Mesh Type	Tetrahedral, Prisms, Pyramids	
Number of elements	Tank-1: 106,417 tetrahedral—90,689 prisms—15,400 pyramids—328	Tank-4: 183,571 tetrahedral—157,611 prisms—25,584 pyramids—376
	Tank-2: 160,991 tetrahedral—145,896 prisms—14,785 pyramids—310	Tank-5: 180,328 tetrahedral—157,609 prisms—22,400 pyramids—319
	Tank-3: 528,070 tetrahedral—453,198 prisms—68,976 pyramids—5896	Tank-6: 632,839 tetrahedral—554,367 prisms—74,712 pyramids—3760
Min element quality	Tank-1: 0.1659	Tank-4: 0.09616
	Tank-2: 0.0973	Tank-5: 0.1144
	Tank-3: 0.09381	Tank-6: 0.09195
Mesh volume, m ³	Tank-1: 2.353	Tank-4: 2.354
	Tank-2: 2.354	Tank-5: 2.354
	Tank-3: 2.354	Tank-6: 2.356

The number and structure of elements for Tank-4 and Tank-5 are approximately the same, as these tanks are geometrically similar. In Tank-1 and Tank-2, the number of prisms and pyramids is roughly the same, but Tank-2 contains more tetrahedral elements due to the presence of an additional solid wall on the cover and bottom. The min element quality metric helps identify the weakest elements in the mesh, providing insight into potential areas where the mesh may require refinement to ensure accurate and reliable simulation results. For most simulations, a minimum element quality of 0.1 or higher is typically considered acceptable. As shown in Table 3, Tank-1 exhibits comparatively better element quality due to its simpler geometry, while the remaining tanks have values close to or equal to 0.1.

The total internal mesh volume for all six tanks was approximately the same. Figure 3 illustrates the computational grids for the more complex Tank-3 and Tank-6, with enlarged sections of the meshes around the perforations. In these performed meshes, the system of equations was discretized using the finite element method (FEM).

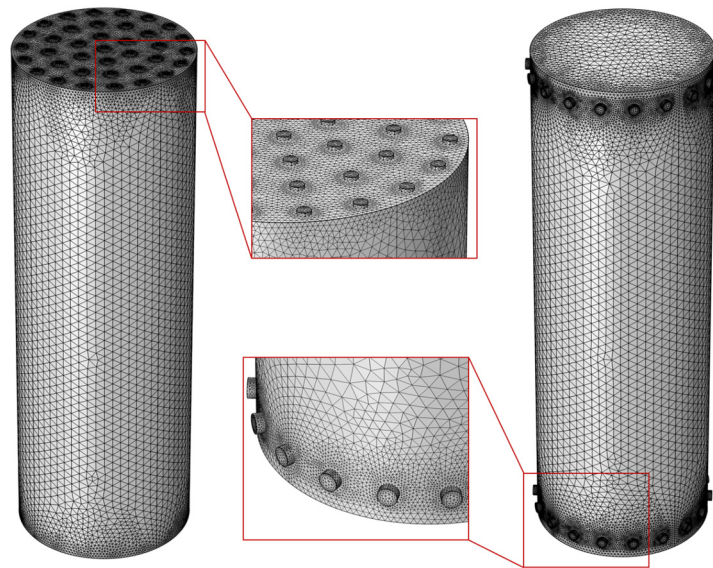


Figure 3. Three-dimensional computational grid for Tank-3 and Tank-6.

Figure 4 shows a graph of the calculation results for grid convergence testing for Tank-1. Four different grid sizes were selected, with 19,573, 55,439, 106,417, and 300,721 element counts. According to the results of the time-dependent temperature distribution at the center of the tank, there was no discernible difference between the last two grids. Therefore, calculations could be performed using the grid with 106,417 elements. A similar grid sensitivity analysis was conducted for the other tanks. The grid sensitivity analysis also indicated that the mesh sizes specified in Table 3 for the six tanks were adequate and did not require further refinement or increased elements.

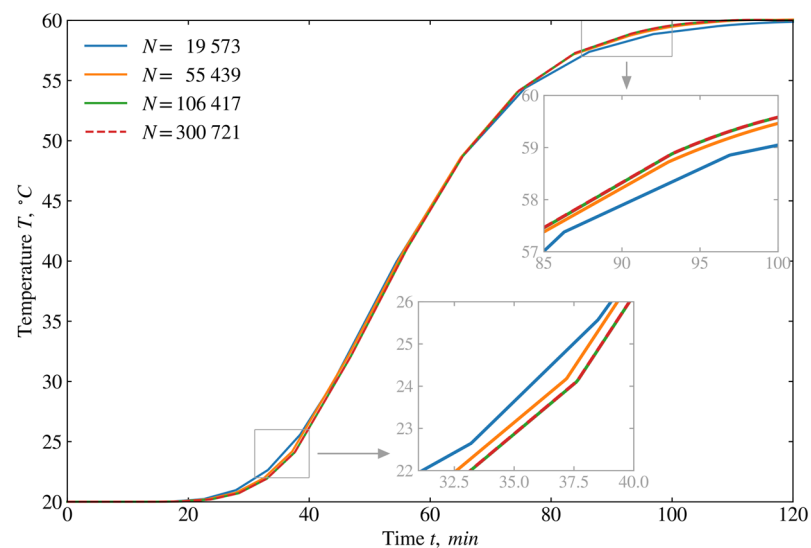


Figure 4. Time evolution of the temperature at the midpoint of Tank-1 on various meshes of increasing size.

4.2. Model Validation

To validate the numerical solver, a comparison was made with the experimental data presented by Zachar et al. [24]. In the study by Zachar et al. [24], a transparent tank was constructed to visually observe the development of a thermocline when dye was injected into the water from an opening at the bottom of the tank, as depicted in Figure 5a. To enhance thermal stratification, a thin, flat plate was placed near the inlet of the tank. For temperature measurements within the tank, 20 temperature sensors were employed along

the height of the tank, positioned between the central axis (along the z-axis) and the right sidewall in the middle section.

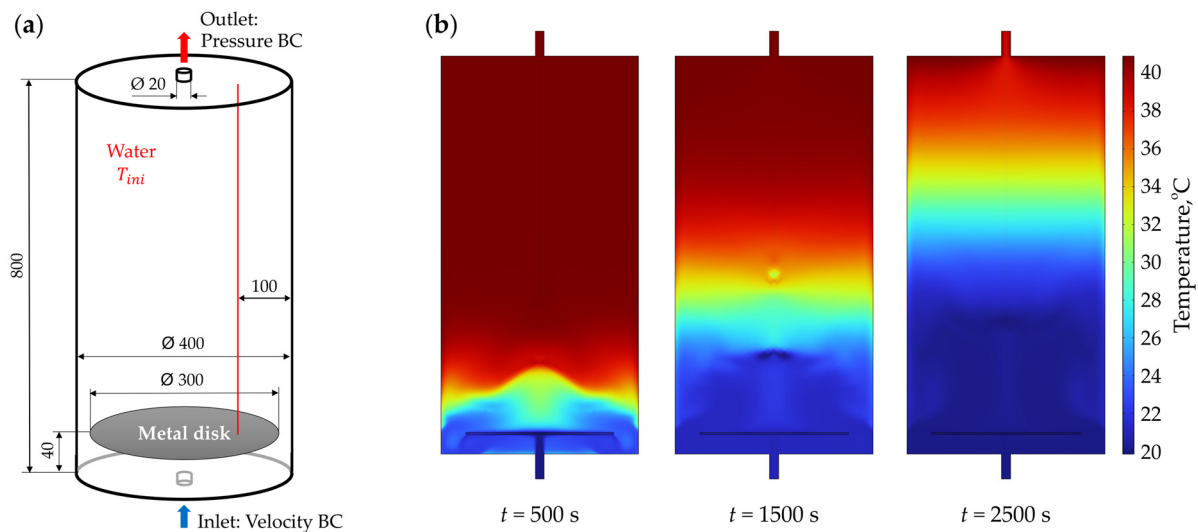


Figure 5. Experimental configuration for validation purposes: (a) 3D diagram; (b) COMSOL results.

The height of the tank was 800 mm, with an internal diameter of 400 mm, while the inlet and outlet nozzles had a diameter of 20 mm. A tree of temperature sensors was positioned 100 mm from the right sidewall. The thin plate had a diameter of 300 mm and was positioned 40 mm above the bottom of the tank. The primary purpose of using this thin disc near the bottom of the tank was to reduce the inlet nozzle velocity, thus allowing the HTF to flow around the plate and improving thermal stratification. The initial water temperature in the tank was 41 °C, while the inlet fluid temperature was 20 °C, with an inlet flow rate of 1.6 L/min [24].

To compare the obtained numerical results with the experimental data, dimensionless parameters for temperature T^* were presented as follows:

$$T^* = \frac{T - T_{in}}{T_{ini} - T_{in}}, \quad (23)$$

Simulations were conducted under these conditions for 2500 s, resulting in the distribution of the dimensionless temperature T^* . Figure 5b presents the effect of injecting cold water at 20 °C on the evolution of static temperature contours between 500 s and 2500 s. In this case, the impact of tank discharging on the thermal stratification layers can be observed. To ensure the accuracy of the results, a comparison with experimental data is necessary.

Figure 6 presents a comparison of the 3D numerical results obtained using COMSOL Multiphysics with the experimental data from Zachar et al. [24], as well as with the 2D numerical results from Bouhal et al. [12] obtained with ANSYS Fluent. These results correspond to 1500 s, as shown in Figure 5b and the experiment by Zachar et al. [24]. Based on a visual inspection of Figure 6, the 3D COMSOL results are closer to the experimental data than the 2D ANSYS results by Bouhal et al. [12]. According to the error analysis between the 3D results and the experimental data, the *RMSE* is 0.1035, indicating a good level of data agreement.

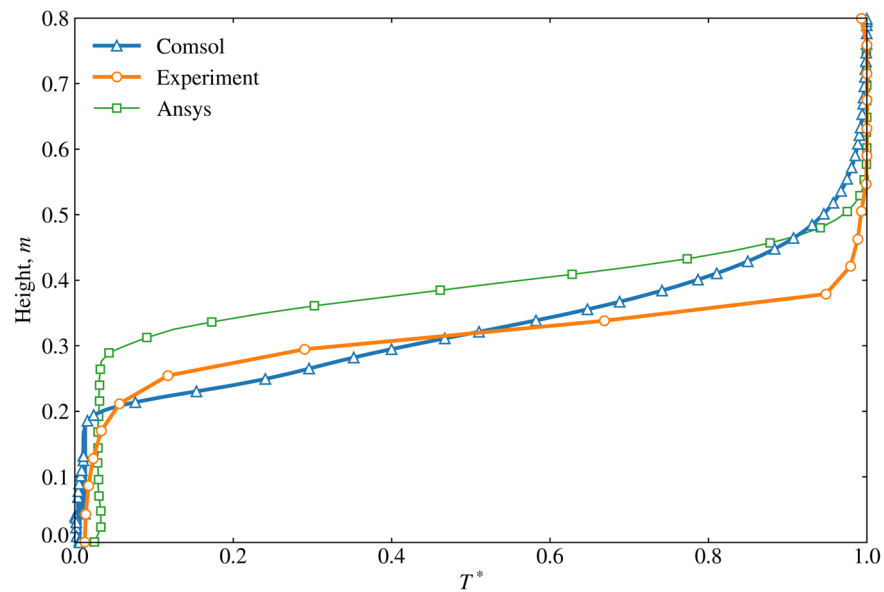


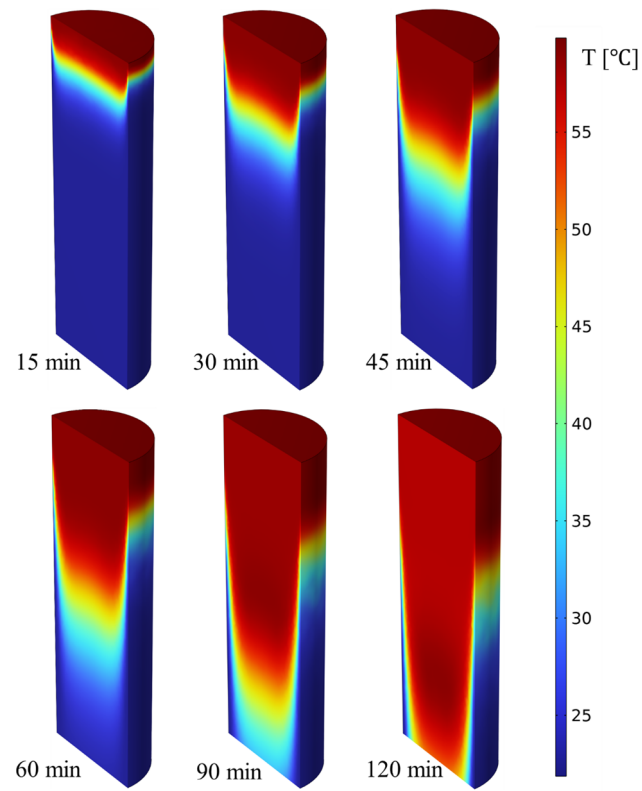
Figure 6. Validation curve showing the progression of dimensionless temperature across the tank's height.

Based on the obtained data, it can be concluded that the 3D numerical simulation algorithm developed using COMSOL Multiphysics accurately describes the processes within the sensible thermal storage tank. This model can be effectively utilized for future simulations involving tanks with different inlet and outlet configurations.

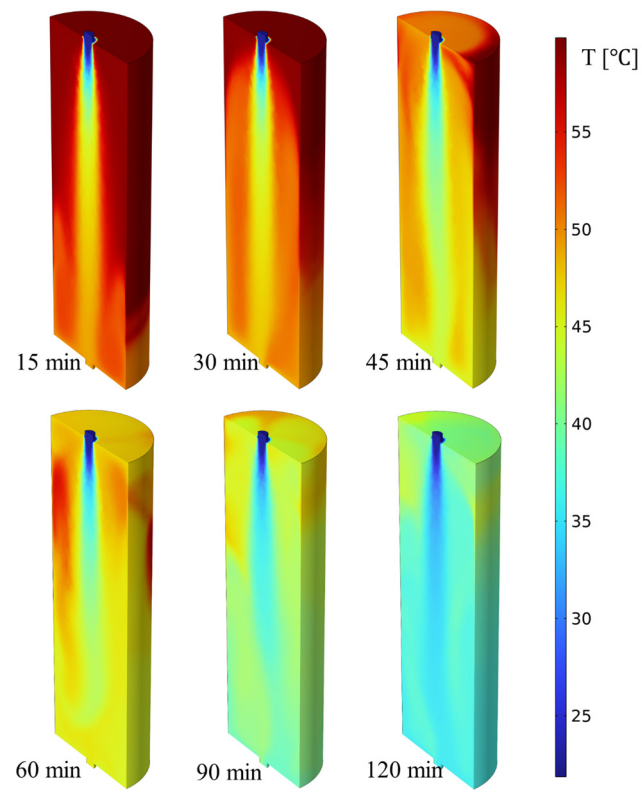
5. Results and Discussion

This section presents the results of the three-dimensional CFD analysis conducted on a hot water storage tank with varying inlet and outlet configurations. This study primarily examines thermal stratification and fluid dynamics during the charging and discharging phases. The findings include detailed temperature distributions, flow patterns, and the influence of different inlet and outlet configurations on the thermal storage efficiency of the tank. Performance metrics for each of the six tank configurations are analyzed, and conclusions are drawn based on the simulation outcomes.

Figure 7 shows the 3D temperature distribution over time within the tanks. The charging mode is depicted for Tank-1, Tank-3, and Tank-5, while the discharging mode is illustrated for Tank-2, Tank-4, and Tank-6. The presented temperature field is measured in degrees Celsius. During the charging process, the heat transfer fluid (HTF) enters from the top of the tank and exits from the bottom. The fluid flow patterns during the charging and discharging modes are symmetric; therefore, the cold HTF enters from the top and exits from the bottom of the tank for discharging. According to the Reynolds number calculation, which is 635, the flow of the incompressible fluid is laminar. Nevertheless, test calculations were conducted with and without the k-e model, an embedded solver in COMSOL for turbulent flows based on the RANS approach. The numerical results show no difference between the laminar and turbulent models. Therefore, all the subsequent calculations were performed using the laminar solver, which also reduces computation time by avoiding the additional RANS model equations. The evolution of the temperature distribution is shown at 15, 30, 45, 60, 90, and 120 min, respectively, for both the charging and discharging modes. The behavior of the HTF inside the tanks for each configuration is nearly symmetrical between the charging and discharging modes. Therefore, the decision was made to display three tanks in the charging mode and three tanks in the discharging mode. The primary objective of illustrating the 3D temperature field is to inspect the flow behavior visually and to select the most optimal configuration based on visual assessment.

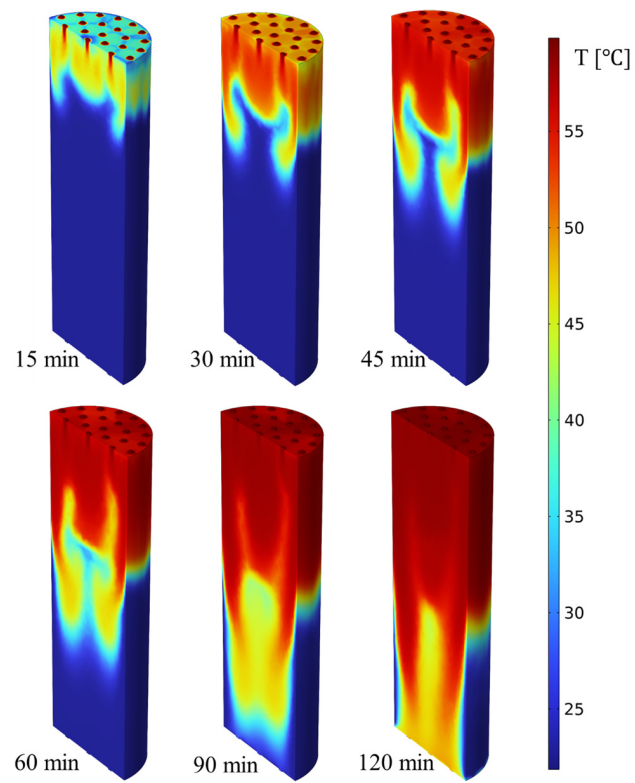


(a)

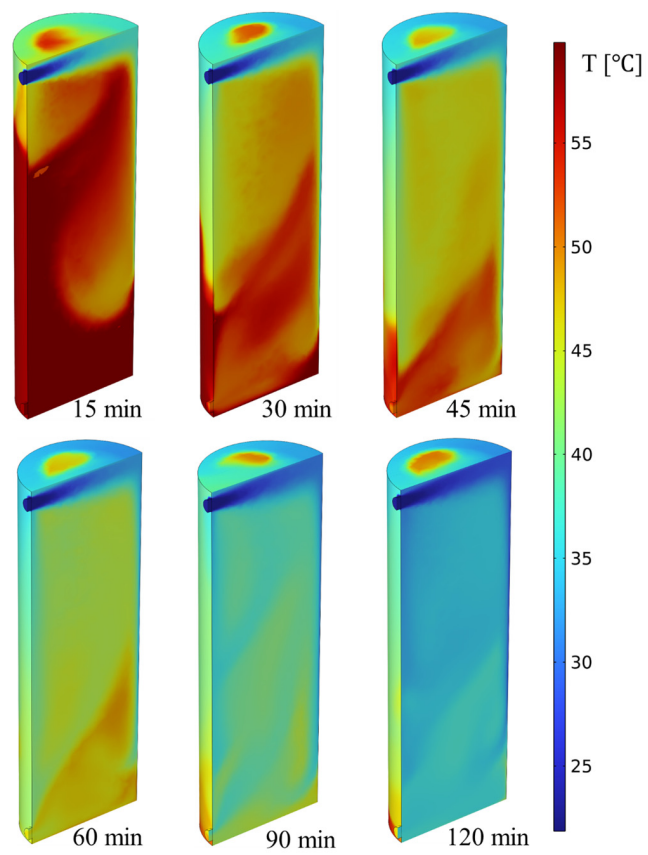


(b)

Figure 7. Cont.

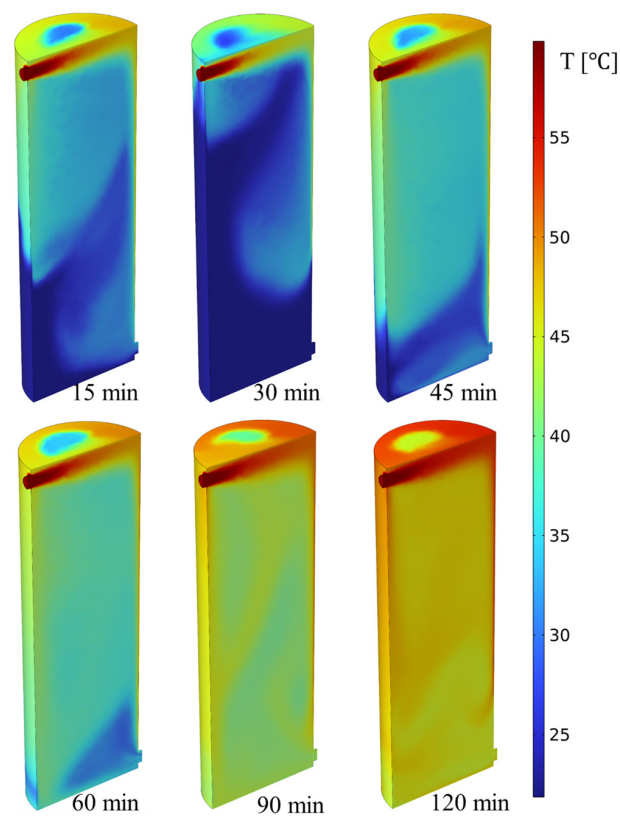


(c)

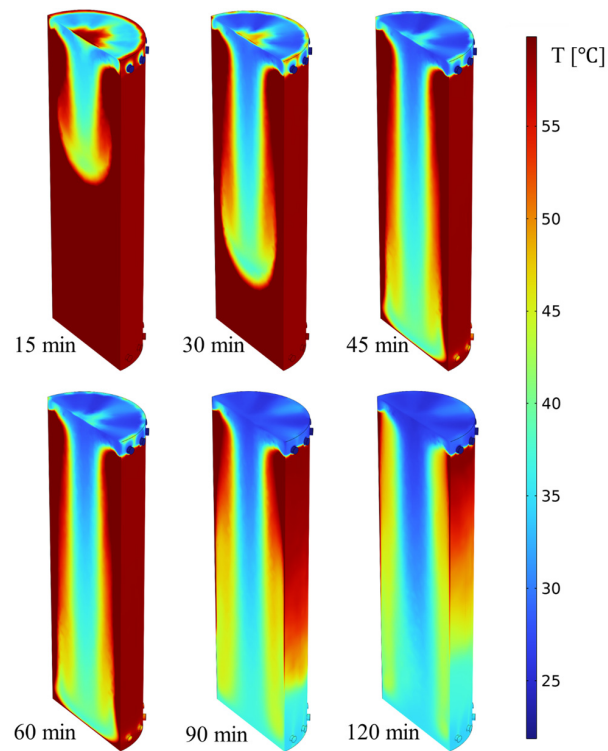


(d)

Figure 7. Cont.



(e)



(f)

Figure 7. Time-dependent temperature distribution of the heat transfer fluid: (a) Tank-1 during the charging mode; (b) Tank-2 during the discharging mode; (c) Tank-3 during the charging mode; (d) Tank-4 during the discharging mode; (e) Tank-5 during the charging mode; (f) Tank-6 during the discharging mode.

As shown in Figure 7a, Tank-1 exhibited a more uniform temperature distribution, and the tank was fully charged without the formation of so-called dead zones, where water remains less heated.

However, implementing a tank with such a large inlet, where the entire top or bottom serves as the inlet for the HTF, is challenging, and it is not feasible to supply such a large volume of heated fluid. This configuration is primarily included for comparative analysis and cannot be recommended for use in tanks containing phase change materials (PCMs).

As stated in the section on initial and boundary conditions, the inlet volumetric flow rate of the HTF remained constant at $0.000327 \text{ m}^3/\text{s}$ for all cases. In Tank-1, the inlet velocity of the HTF was 0.000416 m/s , resulting in a longer charging time for Tank-1, where the slow evolution of the thermocline over time can be observed. In contrast, in Tank-2, using a single nozzle increased the HTF velocity significantly to 0.0416 m/s . As shown in Figure 7b, the colder fluid reached the outlet nozzle quickly, leading to the formation of dead zones where hotter water remained in the tank. Even after 120 min, the temperature of the water in the upper corners of the tank remained around $40 \text{ }^\circ\text{C}$. With this configuration, even at a qualitative level, it is evident that the discharging process is inefficient, and thus, the charging process is also inefficient. The behavior of the incoming water with a single nozzle can be compared to injecting a jet into stationary fluid. Consequently, with such a configuration, phase change materials (PCMs) inside the tank cannot be fully melted during charging, nor fully crystallized during discharging.

Figure 7c shows the temperature distribution in Tank-3 during the charging mode. In this configuration, both the top and bottom of the tank were perforated, and a nozzle system was used. This configuration combines the advantages of both Tank-1 and Tank-2. The inlet velocity of the HTF was 0.00704 m/s . Similar to Tank-1, Tank-3 exhibited uniform heating throughout the tank without the formation of dead zones. It can be observed that the thermocline had a somewhat swirling structure. With this inlet/outlet configuration, the tank can be easily integrated into a hydraulic system. This setup resembles a showerhead configuration, where a smaller diameter pipe transitions to a larger perforated pipe. In future applications, when PCM containers or capsules are placed inside the tank, the multiple nozzles will allow the HTF to flow evenly around these internal obstacles. Based on this preliminary analysis, this configuration can be recommended for use.

Figure 7d,e present the simulation results for Tank-4 and Tank-5. For both configurations, the inlet water velocity was the same as in Tank-2, at 0.0416 m/s . In these cases, the inlet water also behaved like a jet, but unlike Tank-2, Tank-4 and Tank-5 exhibited more uniform mixing, resulting in improved charging and discharging processes. The figures show that the incoming fluid did not reach the outlet nozzle as quickly, which is likely due to the jet impinging on the tank walls, causing recirculation and the formation of vortices. This enhances the mixing of hotter and cooler water and vice versa. While the 3D temperature distribution indicates that, unlike Tank-1 and Tank-3, the temperature at 120 min for Tank-5 was lower, the mixing process in Tank-4 and Tank-5 was significantly better than in Tank-2. Visually, the flow behavior in Tank-4 and Tank-5 appears similar. However, having the inlet and outlet nozzles positioned on opposite sides, as in Tank-5, yielded better results.

Figure 7f presents the numerical results of the temperature distribution for Tank-6 during the discharging mode. During the charging phase, a symmetrical pattern was observed. This configuration was designed to improve upon the performance of Tank-4 and Tank-5. The inlet water velocity from the system of side nozzles was 0.00643 m/s , which is close to that of Tank-3. However, unlike Tank-3, significant dead zones formed in Tank-6. As shown in Figure 7f, when the colder HTF was injected, a cold zone formed in the central part of the tank and gradually moved downward over time. Simultaneously, substantial dead zones formed near the vertical walls of the tank, which persisted even after 120 min of discharging. This configuration appears to degrade the performance.

Based on the visual analysis, Tank 3 is the most promising for further use in thermal storage systems with PCM. This tank is preferred in terms of heat distribution and the

practicality of its configuration. However, visual analysis alone is insufficient. Therefore, the following sections provide performance indicator evaluations that will more rigorously assess the efficiency of the configurations.

The efficiency analysis was conducted according to Equations (9)–(22). Figure 8 presents the results for the capacity ratio, calculated using Equations (9)–(11), and the exergy efficiency, calculated using Equations (12)–(14). The capacity ratio indicates how effectively each configuration can retain heat within the specified temperature range of 20 °C to 60 °C, while exergy serves as a measure of the quality of the stored thermal energy in the tank. According to the results, Tank-1 had the highest capacity ratio at 84.6%, followed by Tank-3 at 70.2%, Tank-6 at 69.3%, Tank-4 at 62.8%, Tank-2 at 62.2%, and Tank-5 at 60.2%. In terms of exergy efficiency, Tank-1 again had the highest value at 72.5%, followed by Tank-3 at 50.5%, Tank-6 at 49.2%, Tank-4 at 40.7%, Tank-2 at 39.8%, and Tank-5 at 37.4%. The order of the tanks is consistent across both parameters.

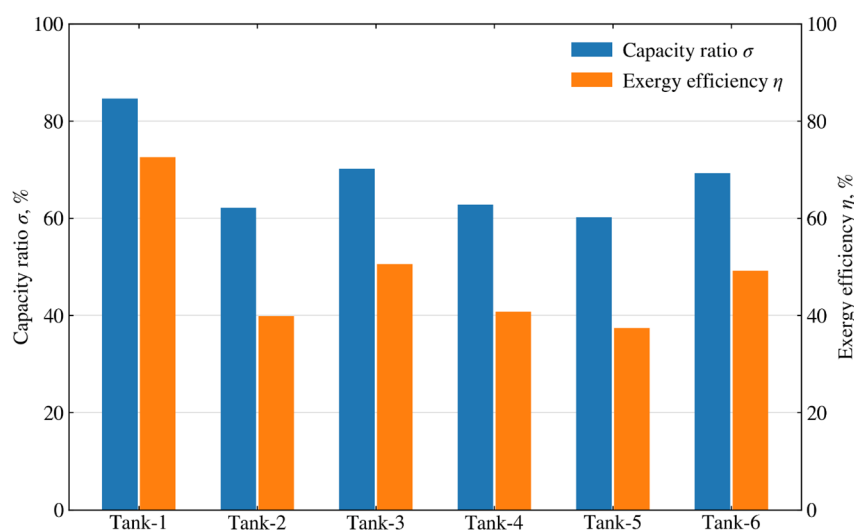


Figure 8. Comparison of capacity ratios and exergy efficiencies for the various tanks.

It is interesting to note that Tank-2 shows better performance than Tank-4 and Tank-5, which was not evident from the visual analysis. Tank-6 had values close to those of Tank-3, although Tank-3 still outperformed it.

Figure 9 presents the charging and discharging efficiency results for the six thermal storage tanks with sensible heat storage, calculated according to Equations (15)–(19). In terms of charging efficiency, Tank-1 ranks highest with a value of 89.7%, followed by Tank-3 at 79.9%, Tank-6 at 77.6%, Tank-2 at 72.9%, Tank-5 at 67.2%, and Tank-4 at 66.5%. It is noteworthy that Tank-2 shows higher charging efficiency than Tank-4 and Tank-5. Table 4 summarizes these results.

The Richardson number, as defined by Equation (21), characterizes the balance between buoyancy and inertial forces within the flow. A higher Richardson number indicates that buoyancy has a greater influence on the flow dynamics. This metric is useful for analyzing the evolution of temperature distribution within the tank and understanding the impact of various parameters on heat transfer efficiency. In simpler terms, a lower Richardson number corresponds to more effective mixing within the fluid. Furthermore, the Richardson number should vary smoothly over time, without any abrupt fluctuations, to ensure stable and predictable flow behavior.

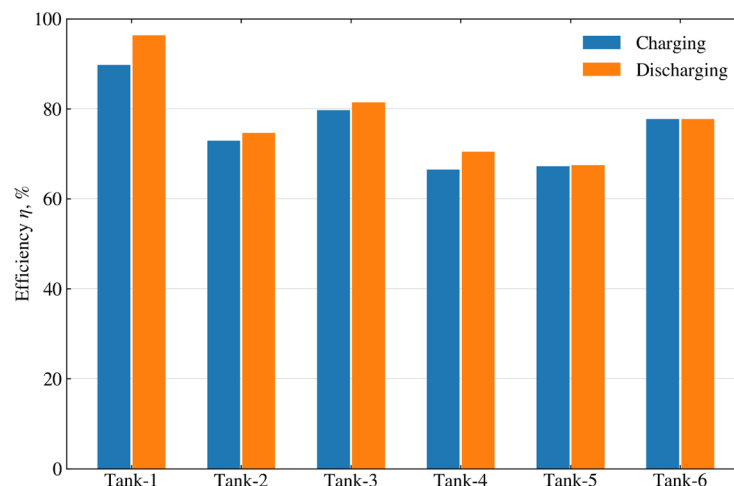


Figure 9. Comparison of charging and discharging efficiencies for the tanks.

Table 4. Performance indicators for the various tanks.

Capacity Ratio	%	Exergy Efficiency	%	Charging Efficiency	%	Discharging Efficiency	%
σ_1	84.6	$\eta_{exergy1}$	72.5	η_{ch1}	89.7	η_{dis1}	96.3
σ_2	62.2	$\eta_{exergy2}$	39.8	η_{ch2}	72.9	η_{dis2}	74.6
σ_3	70.2	$\eta_{exergy3}$	50.5	η_{ch3}	79.7	η_{dis3}	81.4
σ_4	62.8	$\eta_{exergy4}$	40.7	η_{ch4}	66.5	η_{dis4}	70.4
σ_5	60.2	$\eta_{exergy5}$	37.4	η_{ch5}	67.2	η_{dis5}	67.4
σ_6	69.3	$\eta_{exergy6}$	49.2	η_{ch6}	77.6	η_{dis6}	77.7

Figure 10 shows the time distribution of the Richardson number for the six tank configurations. The variation of the Richardson number (Ri) over time on the graph reflects the process of mixing or stratification in each of the tanks. For all the tanks, Ri began at a high value, indicating strong stratification (density separation) within the tank. This suggests that at the start of the process, mixing within the tank was minimal or absent. A decrease in Ri indicates that mixing became more intense over time and stratification decreased. A sharp drop in Ri , as observed in Tank-6, may signify the sudden breakdown of stratification and rapid mixing of the fluid within the tank. Tanks with a gradual decline in Ri (such as Tank-1 and Tank-3) may exhibit steady and progressive mixing. Tanks with sharp fluctuations in Ri (such as Tank-5 and Tank-6) may indicate unstable mixing processes, possibly caused by turbulence or changes in fluid flow velocity. If Ri falls to a low value (below 10), this may suggest nearly complete mixing and the elimination of density stratification.

If the goal is to achieve uniform mixing, tanks with a rapid and stable decline in Ri are preferable. Conversely, if maintaining stratification is important (for example, to preserve a specific temperature layer), Ri must remain high throughout the process. Therefore, the graph provides a means to evaluate the efficiency and nature of mixing in each tank and to select the optimal parameters for controlling this process. In Tank-2, Tank-4, and Tank-5, the single nozzle inlet and outlet configuration generated a high-velocity jet, which induced vortical flow within the tank. This appears to contribute to the oscillatory behavior observed in the Richardson number for these cases, as shown in Figure 10. These oscillations suggest uneven mixing within these tanks. Consequently, the Richardson number analysis further validates that Tank-1 and Tank-3 are the most suitable configurations for achieving uniform temperature distribution within the tank.

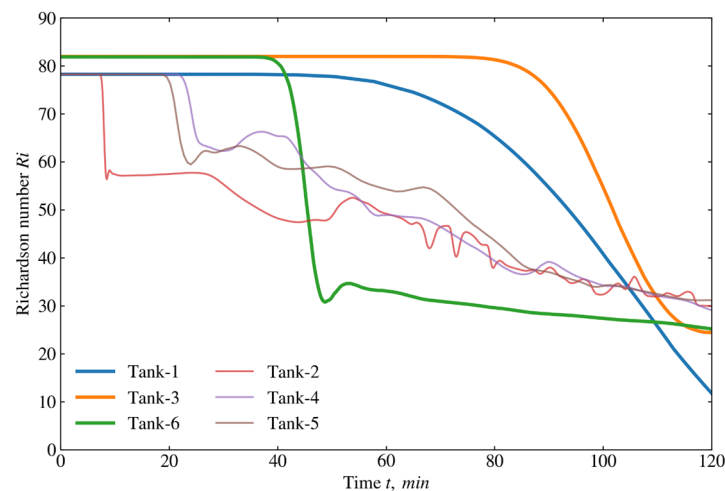


Figure 10. Time evolution of the Richardson number for the tanks.

The analysis of fundamental dimensionless parameters, as presented in Equation (22), indicates that the flow is laminar for all six tanks, as the Reynolds number, calculated based on the volumetric flow rate, is 635—below the threshold of 2000 typically used for fluid flow in pipes. The Prandtl number was determined to be approximately 4.5 at the given temperature, and the corresponding Peclet number was calculated as 2858 for all the configurations. For analyzing sensible heat storage in a tank, the Peclet number is essential for identifying the dominant heat transfer mechanism—whether convection or conduction. When $Pe \gg 1$, this signifies that convective heat transfer greatly exceeds thermal conductivity, meaning that most heat is transported by the fluid flow rather than by thermal conduction within the medium. This is expected, as either warm or cold fluid is introduced into the tank depending on the charging or discharging mode.

6. Conclusions

This study presents an in-depth 3D numerical analysis of six hot water storage tank configurations, evaluating their effectiveness in achieving uniform temperature distribution, strong thermal stratification, and efficient heat retention, with potential applications to systems involving phase change materials (PCMs). Using COMSOL Multiphysics, this study analyzed various inlet and outlet configurations, focusing on performance metrics, such as the Richardson number, capacity ratio, and exergy efficiency.

The key findings from the analysis are summarized as follows:

- Tank-3 demonstrated high efficiency, with a capacity ratio of 0.93 and an exergy efficiency of 85%, indicating effective stratification and temperature distribution. Tank-1 achieved slightly better metrics (capacity ratio of 0.95 and exergy efficiency of 87%) but is less practical for real-world implementation.
- The Reynolds (635), Prandtl (4.5), and Peclet (2858) numbers confirmed laminar flow across all the configurations, with a dominant convective heat transfer influence, facilitating efficient heat transport within the tanks.
- Tank-3's configuration, with perforations on the top and bottom, yielded a stable temperature profile suited for PCM integration, ensuring consistent flow around vertical PCM containers and facilitating thorough charging and discharging.

These results offer valuable insights for the design of efficient thermal storage systems, particularly in renewable energy applications requiring precise temperature control. The Tank-3 configuration, with its stable and uniform heat distribution, is especially promising for integrating PCMs, enhancing energy density and storage efficiency in practical applications.

Future studies should explore not only the integration of PCM containers but also the application of this configuration to heat pump water heaters, solar water heaters with

sensible heat storage, and high-temperature heat storage systems using various working fluids. Examining the effects of different flow rates, PCM materials, and tank geometries would further refine model accuracy. Additionally, experimental validation with PCMs and other storage systems, including those operating with high-temperature fluids, would provide comprehensive insights into the practicality of these configurations under diverse operating conditions.

Author Contributions: Conceptualization, Y.B., O.B., A.K. and M.K.; methodology, A.T., Y.B., O.B. and A.K.; software, A.A., A.S., Y.B. and O.B.; validation, A.A., A.S. and Y.B.; formal analysis, A.A., A.S., A.T. and Y.B.; investigation, A.A., A.S., Y.B. and O.B.; resources, Y.B., O.B., A.K. and M.K.; data curation, A.A., A.S. and Y.B.; writing—original draft preparation, A.A. and Y.B.; writing—review and editing, Y.B., O.B., A.K. and M.K.; visualization, A.A. and A.S.; supervision, Y.B., O.B., A.K. and M.K.; project administration, Y.B., O.B. and A.K. All authors have read and agreed to the published version of the manuscript.

Funding: This research was funded by the Committee of Science of the Ministry of Science and Higher Education of the Republic of Kazakhstan, Grant No. AP14872287 “Study of Cascade Solar Thermal Energy Storage Efficiency Using Phase Change Materials in Continental Climate”.

Data Availability Statement: The original contributions presented in the study are included in the article, further inquiries can be directed to the corresponding authors.

Acknowledgments: The authors express their gratitude for the support provided by the “Heat Management” team from the LEMTA R&D Center of the University of Lorraine and CNRS, France and the Postdoctoral Research Programme for Yerzhan Belyayev at Al-Farabi Kazakh National University, Almaty, Kazakhstan. We would like to thank the organizers of the double-degree program between Al-Farabi Kazakh National University (Kazakhstan) and the University of Lorraine (France) in the specialty “7M05405—Mechanics and Energy” for their contribution to the preparation of master’s graduates.

Conflicts of Interest: The authors declare no conflicts of interest.

Nomenclature

\vec{u}	Velocity vector;
u_r, u_θ, u_z	Velocity components, m/s;
ρ	Density, kg/m ³ ;
p	Pressure, Pa;
ν	Kinematic viscosity, m ² /s;
\vec{g}	Gravity, m/s ² ;
β	Coefficient of thermal expansion;
\dot{m}	Mass flow rate, kg/s;
C_p	Heat capacity, J/kg °C;
T	Temperature, °C;
T^*	Dimensionless temperature;
Q	Flow rate, m ³ /s;
σ	Capacity ratio, %;
E	Energy, J;
V	Volume, m ³ ;
η	Exergy, charging, discharging efficiency, %;
t	Time, s;
k	Thermal conductivity, W/mK;
α	Thermal diffusivity, m ² /s;
Ri	Richardson number;
Pe	Peclet number;
D	Diameter of tank, m;
b	Diameter of inlet/outlet nozzles, m;
H	Height of tank, m;
$error$	Relative error;

Subscripts

f	Heat transfer fluid;
z	Vertical direction;
θ	Azimuthal direction;
r	Radial direction;
h	Hot water;
c	Cold water;
ini	Initial value;
in	Inlet quantity;
out	Outlet quantity;
top	Top layer;
bottom	Bottom layer;
exp	Experimental value;
num	Numerical value;

Abbreviations

TES	Thermal energy storage;
SHS	Sensible heat storage;
LHS	Latent heat storage;
PCM	Phase changing material;
BC	Boundary conditions;
HTF	Heat transfer fluid;
CFD	Computational fluid dynamics;
H&M	Heat and mass transfer;
FDM	Finite difference method;
FEM	Finite element method;
FVM	Finite volume method;

References

- Faraj, K.; Khaled, M.; Faraj, J.; Hachem, F.; Castelain, C. A review on phase change materials for thermal energy storage in buildings: Heating and hybrid applications. *J. Energy Storage* **2021**, *33*, 101913. [[CrossRef](#)]
- Wang, H.; Xie, B.; Li, C. Review on operation control of cold thermal energy storage in cooling systems. *Energy Built Environ.* **2024**, *in press*. [[CrossRef](#)]
- Li, G.; Zheng, X. Thermal energy storage system integration forms for a sustainable future. *Renew. Sustain. Energy Rev.* **2016**, *62*, 736–757. [[CrossRef](#)]
- Chekifi, T.; Boukraa, M. CFD applications for sensible heat storage: A comprehensive review of numerical studies. *J. Energy Storage* **2023**, *68*, 107893. [[CrossRef](#)]
- Diaconu, B.M.; Cruceru, M.; Anghelescu, L. A critical review on heat transfer enhancement techniques in latent heat storage systems based on phase change materials. Passive and active techniques, system designs and optimization. *J. Energy Storage* **2023**, *61*, 106830. [[CrossRef](#)]
- Gautam, A.; Saini, R.P. A review on sensible heat based packed bed solar thermal energy storage system for low temperature applications. *Sol. Energy* **2020**, *207*, 937–956. [[CrossRef](#)]
- Varthani, A.J.; Shastri, S.; Baljit, S.; Kausalyah, V. A systematic review of metal foam and heat pipe enhancement in Latent Heat Thermal Energy Storage System. *J. Energy Storage* **2022**, *56*, 105888. [[CrossRef](#)]
- Chandra, Y.P.; Matuska, T. Stratification analysis of domestic hot water storage tanks: A comprehensive review. *Energy Build.* **2019**, *187*, 110–131. [[CrossRef](#)]
- Lou, W.; Fan, Y.; Luo, L. Single-tank thermal energy storage systems for concentrated solar power: Flow distribution optimization for thermocline evolution management. *Energy Storage* **2020**, *32*, 101749. [[CrossRef](#)]
- Al-abidi, A.A.; Mat, S.B.; Sopian, K.; Sulaiman, M.Y.; Abdulrahman, T.M. CFD applications for latent heat thermal energy storage: A review. *Renew. Sustain. Energy Rev.* **2023**, *20*, 353–363. [[CrossRef](#)]
- Hosseinnia, S.M.; Akbari, H.; Sorin, M. Numerical analysis of thermocline evolution during charging phase in a stratified thermal energy storage tank. *J. Energy Storage* **2021**, *40*, 102682. [[CrossRef](#)]
- Bouhal, T.; Fertahi, S.; Agrouaz, Y.; El Rhafiki, T.; Kousksou, T.; Jamil, A. Numerical modeling and optimization of thermal stratification in solar hot water storage tanks for domestic applications: CFD study. *Sol. Energy* **2017**, *157*, 441–455. [[CrossRef](#)]
- Fertahi, S.E.; Bouhal, T.; Kousksou, T.; Jamil, A.; Benbassou, A. Experimental study and CFD thermal assessment of horizontal hot water storage tank integrating Evacuated Tube Collectors with heat pipes. *Sol. Energy* **2018**, *170*, 234–251. [[CrossRef](#)]
- Lou, W.; Xie, B.; Aubril, J.; Fan, Y.; Luo, L.; Arrivé, A. Optimized flow distributor for stabilized thermal stratification in a single-medium thermocline storage tank: A numerical and experimental study. *Energy* **2023**, *263 Pt A*, 125709. [[CrossRef](#)]

15. Kumar, K.; Singh, S. Investigating thermal stratification in a vertical hot water storage tank under multiple transient operations. *Energy Rep.* **2021**, *7*, 7186–7199. [[CrossRef](#)]
16. Shafieian, A.; Bahrami, H.R.; Roostaei, A.; Feyzi, S.S. Effects of different inlet configurations on the performance of solar storage tanks: A three-dimensional unsteady CFD simulation. *Case Stud. Therm. Eng.* **2023**, *45*, 103019. [[CrossRef](#)]
17. Kong, L.; Yuan, W.; Zhu, N. CFD Simulations of Thermal Stratification Heat Storage Water Tank with an Inside Cylinder with Openings. *Procedia Eng.* **2016**, *146*, 394–399. [[CrossRef](#)]
18. Wang, M.; Hu, E.; Chen, L. CFD analysis and optimization of thermal stratification in a Thermal Diode Tank (TDT). *J. Energy Storage* **2024**, *76*, 109837. [[CrossRef](#)]
19. Shaikh, W.; Wadegaonkar, A.; Kedare, S.B.; Bose, M. Numerical simulation of single media thermocline based storage system. *Sol. Energy* **2018**, *174*, 207–217. [[CrossRef](#)]
20. COMSOL. *COMSOL Multiphysics*, Version 5.6; COMSOL: Burlington, MA, USA, 2020.
21. Lou, W.; Luo, L.; Hua, Y.; Fan, Y.; Du, Z. A review on the performance indicators and influencing factors for the thermocline thermal energy storage systems. *Energies* **2021**, *14*, 8384. [[CrossRef](#)]
22. Li, G. Sensible heat thermal storage energy and exergy performance evaluations. *Renew. Sustain. Energy Rev.* **2016**, *53*, 897–923. [[CrossRef](#)]
23. Shah, L.J.; Furbo, S. Entrance effects in solar storage tanks. *Sol. Energy* **2003**, *75*, 337–348. [[CrossRef](#)]
24. Zachár, A.; Farkas, I.; Szlivka, F. Numerical analyses of the impact of plates for thermal stratification inside a storage tank with upper and lower inlet flows. *Sol. Energy* **2003**, *74*, 287–302. [[CrossRef](#)]

Disclaimer/Publisher’s Note: The statements, opinions and data contained in all publications are solely those of the individual author(s) and contributor(s) and not of MDPI and/or the editor(s). MDPI and/or the editor(s) disclaim responsibility for any injury to people or property resulting from any ideas, methods, instructions or products referred to in the content.